Some experimental observations of crack-tip mechanics with displacement data

M. Mokhtari, P. Lopez-Crespo, B. Moreno
Department of Civil and Materials Engineering, University of Malaga, C/Dr. Ortiz Ramos s/n, 29071 Malaga, Spain
plopezcrespo@uma.es

M. Zanganeh
ORAU, Oak Ridge, TN, USA
mohammad.zanganehgheshlaghi@nasa.gov

ABSTRACT. In the past two decades, crack-tip mechanics has been increasingly studied with full-field techniques. Within these techniques, Digital Image Correlation (DIC) has been most widely used due to its many advantages, to extract important crack-tip information, including Stress Intensity Factor (SIF), Crack Opening Displacement, J-integral, T-stress, closure level, plastic zone size, etc. However, little information is given in the literature about the experimental setup that provides best estimations for the different parameters. The current work aims at understanding how the experimental conditions used in DIC influence the crack-tip information extracted experimentally. The influence of parameters such as magnification factor, size of the images, position of the images with respect the crack-tip and size of the subset used in the correlation is studied. The influence is studied in terms of SIF and T-stress by using Williams' model. The concept of determination of the K-dominance zone from experimental data has also explored. In this regard, cyclic loading on a fatigue crack in a compact tension (CT) specimen, made of aluminium 2024-T351 alloy, has been applied and the surface deformation ahead of the crack tip has been examined. The comparison between theoretical and experimental values of K_I showed that the effect of subset size on the measured K_I is negligible compared to the effect of size of the image.

KEYWORDS. Digital image correlation; Stress intensity factor; T-stress; Crack tip displacement field.

INTRODUCTION

Since 1980s in which a group of researchers at the University of South Carolina [1-3] developed the digital image correlation (DIC) method for obtaining the full-field in-plain deformation of an object directly, a growing number of researches has been done to modify the method and its parameters. In brief, DIC compromises of three sequences including 1) sample preparation, 2) taking images before and after loading from the surface of the specimen, and finally 3) calculating displacement and strain information by image processing [4]. DIC is a straight forward, low cost and simple method to measure experimentally surface deformation data with few advantages compared to other full-field

techniques such as Moiré interferometry, photoelasticity and thermoelasticity [4-8]. Experimentally, DIC measurement accuracy can be affected by several factors, such as sub-pixel optimization algorithm, subset size, image quality, etc.[4]. It should be noted here that "subset" refers to an area in the image in which the displacement between images is tracking. Some of the errors introduced by DIC measurements have been estimated by researchers. For example, Fazzini et al. [9] have studied the errors caused by different bit depths of the image, image saturation in respect with subset size, speckle pattern and subset shape function on synthetic images. They found that decreasing the encoding of the images and overexpose of the speckle deteriorate the measurements by a factor of 2 and 10 respectively. In addition, systematic errors due to intensity interpolation, under-matched subset shape function and over-matched subset shape functions have been calculated by Shreier et al. [10, 11] and Yu et al. [12] respectively.

Since the initial works on DIC, algorithms for displacement and strain measurement have been improved and so have the different methods for estimating SIF from DIC data. Most works estimate SIF by fitting numerical functions (such as Westergaard's, Willialms' or Muskhilishvili's series developements) to experimental data [8, 13-15]. Earlier works developed in 1980s used a least-square error analysis procedure in order to estimate the SIF [1, 16]. Subsequently SIF were estimated for fatigue cracks grown in steel by introducing an enriched crack kinematics in cyclic fatigue based on conventional and integrated DIC techniques [17]. Later, a similar methodology was used to evaluate mixed-mode SIF on a crack emanating form a fastener hole [18]. In addition, other more comprehensive models have been proposed to account driving and retarding forces on the crack-tip [19]. Vanladuit et al. [20] introduced a post-processing method for measuring the crack length, crack tip position and stress intensity factors automatically from displacement field. They have validated their methodology by performing a fatigue crack propagation test on an aluminum U-profile. However, it is well known that there is a small region quite close to crack tip, called K-dominance zone, where stress field can be effectively described by stress intensity factor merely. Beyond this annular region, to characterize the crack tip field, the higher order terms (non-singular part of stress field) must be considered. Sun et al. [17], has evaluated the size of K-dominance for a plexiglass. They considered not only the singular but also the nonsingular part of stress fields in order to predict the fracture of the material precisely. In spite of all these efforts for optimizing DIC and related post processing procedures, it seems that the effect of the size of the DIC image fitted to the analytical model has been neglected. In optic literature, the size of the DIC image is studied through the field of view (FOV) and is defined as the angular extent for a given scene imaged by a camera [21]. Since the FOV determines the number and position of data points for a constant subset size, the FOV must be taken into consideration as key parameter for SIF evaluation from DIC data. Finally, the the K-dominance zone has been studied experimentally with the help of higher orders in Williams' series.

MATERIALS AND METHODS

Experiments were conducted on a 2024-T351 aluminum plate. This was machined to obtain a CT specimen according to ASTM E-647 standards [22]. Fig. 1 illustrates the specimen geometry and dimensions. The mechanical properties of the material are summarised in Tab. 1. The sample surface was scratched by abrasive 240, 380 and 800 grit SiC grinding paper to achieve the a random grey intensity distribution required by DIC technique. Cyclic loading was applied with a 100kN Instron servo-hydraulic testing machine. The specimen was fatigue pre-cracked under mode I at a frequency of 10 Hz, load ratio (R) 0.1 and constant stress intensity range (K_{min}/K_{max}) of 10.1 MPa$\sqrt{m}$. After 980,000 cycles the measured crack length was 28.6 mm (a/W = 0.57). An 8-bit 2452×2052 pixels CCD camera coupled with Navitar lens with magnification ranging from 7X to 0.35X and a ring light illumination was used to take images for DIC (Fig. 2). Higher magnification images were acquired with a Questar QM-100 lens (magnification of 9X). In order to achieve larger field of view, macro images were also taken using a macro lens 0.25X. A Questar 3-axis stage was also used to mount and adjust the camera position precisely. The different lenses combinations were used to obtain FOVs ranging from 0.5×0.5 mm² to 20×20 mm². In order to acquire sufficient number of images, the loading rate was reduced to 0.1 Hz while capturing the images.

Young modulus	Yield Stress	UTS	Elongation	Brinell Hardness
73 GPa	325 MPa	470 MPa	20%	137

Table 1: Mechanical properties of 2024-T351 aluminium alloy.

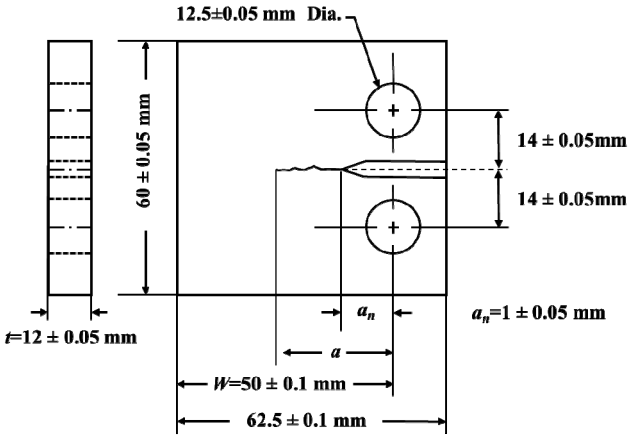

Figure 1: Geometry of the test CT specimen [19].

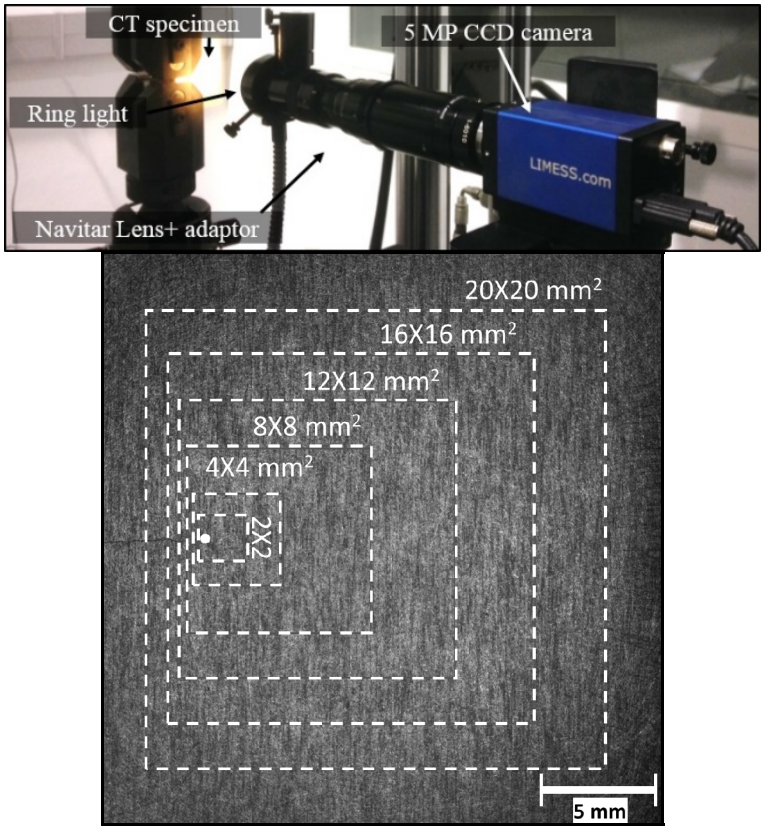

Figure 2.Imaging set up and selected AOIs for a constant field of view. The white point highlights the crack tip location.

In this way, 48 images were acquired each cycle during the loading and unloading of the cycle. Images were captured in seven different magnifications. Subsequently the images were processed with Vic-2D software to obtain the displacement fields. Each image was compared to the initial reference image at P_{min}. The subset centre distance (step size) was set to 1/4 of the subset size in order to achieve independent and non-repetitive data. A high-order interpolation scheme of optimized 8-tap spline was used to achieve sub-pixel accuracy. The correlation criterion was set to zero-normalized sum of squared differences which is insensitive to offset and scale in lighting [21]. The standard deviation confidence interval (E), the confidence interval for matching the points in subsets, was confined lower than 4%. To study the effect of the area of interest (AOI) on the SIF, six different AOIs in a constant FOV were analysed (Fig. 2).
Displacement fields obtained by DIC were then substituted into Williams' series [8]:

$$ModeI\begin{cases} u_I = \sum_{n=1}^{\infty} \frac{r^{\frac{n}{2}}}{2\mu} a_n \left\{ \left[\kappa + \frac{n}{2} + (-1)^n \right] \cos\frac{n\theta}{2} - \frac{n}{2}\cos\frac{(n-4)\theta}{2} \right\} \\ v_I = \sum_{n=1}^{\infty} \frac{r^{\frac{n}{2}}}{2\mu} a_n \left\{ \left[\kappa - \frac{n}{2} - (-1)^n \right] \sin\frac{n\theta}{2} + \frac{n}{2}\sin\frac{(n-4)\theta}{2} \right\} \end{cases} \quad (1)$$

and

$$ModeII\begin{cases} u_{II} = -\sum_{n=1}^{\infty} \frac{r^{\frac{n}{2}}}{2\mu} b_n \left\{ \left[\kappa + \frac{n}{2} - (-1)^n \right] \sin\frac{n\theta}{2} - \frac{n}{2}\sin\frac{(n-4)\theta}{2} \right\} \\ v_{II} = \sum_{n=1}^{\infty} \frac{r^{\frac{n}{2}}}{2\mu} b_n \left\{ \left[\kappa - \frac{n}{2} + (-1)^n \right] \cos\frac{n\theta}{2} + \frac{n}{2}\cos\frac{(n-4)\theta}{2} \right\} \end{cases} \quad (2)$$

where u and v are horizontal and vertical displacements in mode I, μ is the shear modus and $\kappa = (3-\nu)/(1+\nu)$ for plane stress and $\kappa = 3-4\nu$ for plane strain condition, ν is the Poisson's ratio, r and θ are radial and phase distance from the crack, a and b are constant.

Eq. 1 and 2 can be written in terms of the stress intensity factors and T-stress as follows:

$$u = \frac{K_I}{2\mu}\sqrt{\frac{r}{2\pi}}\cos\frac{\theta}{2}(\kappa - 1 + 2\sin^2\frac{\theta}{2}) + \frac{K_{II}}{2\mu}\sqrt{\frac{r}{2\pi}}\sin\frac{\theta}{2}(\kappa + 1 + 2\cos^2\frac{\theta}{2}) + \frac{T}{8\mu}r(\kappa+1)\cos\theta \quad (3)$$

$$v = \frac{K_I}{2\mu}\sqrt{\frac{r}{2\pi}}\sin\frac{\theta}{2}(\kappa + 1 - 2\cos^2\frac{\theta}{2}) - \frac{K_{II}}{2\mu}\sqrt{\frac{r}{2\pi}}\cos\frac{\theta}{2}(\kappa - 1 - 2\cos^2\frac{\theta}{2}) + \frac{T}{8\mu}r(\kappa-3)\sin\theta \quad (4)$$

by using

$$K_I = a_1\sqrt{2\pi}, \quad K_{II} = -b_1\sqrt{2\pi}, \quad T = 4a_2 \quad (5)$$

where K_I and K_{II} are mode I and II of stress intensity factor respectively and T represents T-stress. The effects of addition of non-singular terms of Williams' solution on the experimental and numerical data fitting was also explored. The number of terms increased until the best displacement fit reach and the value of SIFs become stable.

In order to compare the experimental results with the theoretical estimations, the theoretical value of K_I for CT specimen was calculated with the following equations [23]:

$$K_I = \frac{P}{tW^{\frac{1}{2}}}.f_1(\alpha), \qquad \alpha = \frac{a}{W} \quad (6)$$

$$f_1(\alpha) = \frac{(2+\alpha)(0.886 + 4.64\alpha - 13.32\alpha^2 + 14.72\alpha^3 - 5.6\alpha^4}{(1-\alpha)^{3/2}} \quad (7)$$

where a and t are crack length and thickness of sample respectively. The accuracy of experimental results was then examined by introducing a parameter, δ, which is the difference between experimental and theoretical measurements:

$$\delta = |\ K_I \text{ experimental} - K_I \text{ theoretical}\ | \quad (8)$$

Lower δ will be indicative of more accurate estimations of K_I.

Results and Discussion

Fig. 3 illustrates how the standard deviation confidence interval (E) and δ are change with increasing the subset size. It can be seen that although E is reduced by increasing the subset size, no considerable change is observed in δ. This behaviour can be attributed to the surface pattern. In other words, scratching the surface by different grades of abrasive paper, provides sufficient intensity gradients in each subset, even for the smallest one, 19 pixel. However, caution must be taken in subset size selection especially in case of using speckle patterns. Although the large subset size

leads to lower displacement uncertainty, underlying deformation field undergoes incorrect estimation. On the other hand, heterogeneity of displacement fields requires small subset size [17]. Too small subsets, however, increase the random errors [24]. Hild et al. [13], showed that there is a reverse power law relation between E and subset size. Therefore, it has been stated that there is a trade-off between using large and small subset size [4]. Nevertheless, subset sizes ranging from 19 to 151 pixel (equal to the displacement vectors of 39 to 311 micron) have not had significant effect on SIFs measurements in this study.

The effect of considering different number of Williams' solution terms on the quality of fitted data to the experimental displacement for a FOV of 8×8 mm² is shown in Fig. 4. Figs. 4e and 4f show that after 10 terms not only the SIFs and T-stress values have converged, but the data also are fitted very well to the analytical model.

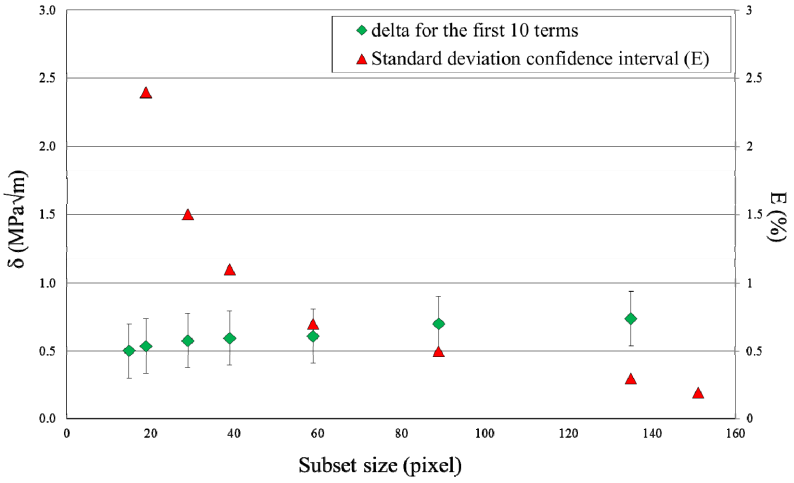

Figure 3. δ as a function of subset size in the magnification of 0.75X.

To have a better understanding of the effect of the number of considered terms on SIFs estimations, the value of δ has been plotted as a function of FOV (Fig. 5). There are two main points in this figure. First, the addition of the second term, T-stress, has not considerable effect on the estimated SIF. In addition, the 10-terms solution provides more accurate estimation of K_I than the 1 or 2-terms solutions. This is more significant for fields of view larger than 8×8 mm². In fact, while the average difference between the 1 and 10-terms estimation of K_I in small fields of view (0.5×0.5 and 1.2×1.2 mm²) are 0.22 MPa√m, it increases to the average value of 0.98 MPa√m for FOVs larger than 8×8 mm². This can be inferred by recalling the fact that the area in the immediate vicinity of the crack-tip is a singular area, where asymptotic singular solutions, K and T terms, can represent the stress state alone [24, 25].

Increasing the size of the field of view and thereby using data points far from the crack-tip, means that higher order terms need to be considered to characterise the crack-tip fields. This idea can be used to estimate experimentally the K-dominance zone from DIC data. In this study, at least 10 terms of Williams' solution need to be considered in FOVs larger than 8×8 mm² to obtain accuracy smaller than 0.5 MPa√m.

Different AOIs can be selected for each FOV. Since AOI determines the number and location of data points as well as FOV, the AOI directly affects the SIF's measurements. Hence, the effect of AOI on SIF is investigated in Fig. 6. The aim is to find out if the same sized FOVs and AOIs will result in a similar estimation of SIFs or not. In this regard, Fig. 6 shows the value of δ as a function of the different FOVs and corresponding AOIs which have been shown in Fig. 2. The interesting point in this figure is that the same-sized FOV and AOI leads to almost the same SIFs estimation. Therefore, one can measure the SIF by selecting a small AOI in an image with low magnification (large FOV). In this way, not only there is no need for high magnifying lenses, but the number of data points that needs to be analysed can also be reduced.

CONCLUSION

The displacement field analysis ahead of a fatigue crack illustrates that the FOV is an effective parameter in measuring the SIF from displacement fields derived from DIC and thus should be reported in test procedures. It was highlighted that subset sizes ranging from 19 to 151 pixel have no considerable effect on measured SIFs in the FOV ranging from 2×2mm² to 20×20 mm². It also was observed that the same-sized FOV and AOI leads to almost the

same estimation of K_I. Therefore, in order to obtain a reliable experimental estimation of SIF (accuracy less than 0.5 MPa√m) from displacement data measured by DIC of aluminium 2014-T351 alloy, one can choose the FOV ranging from 8×8 to 20×20 mm² with an arbitrary subset size ranging from 19 to 151 pixel for a scratched surface of a fatigue cracked CT specimen.

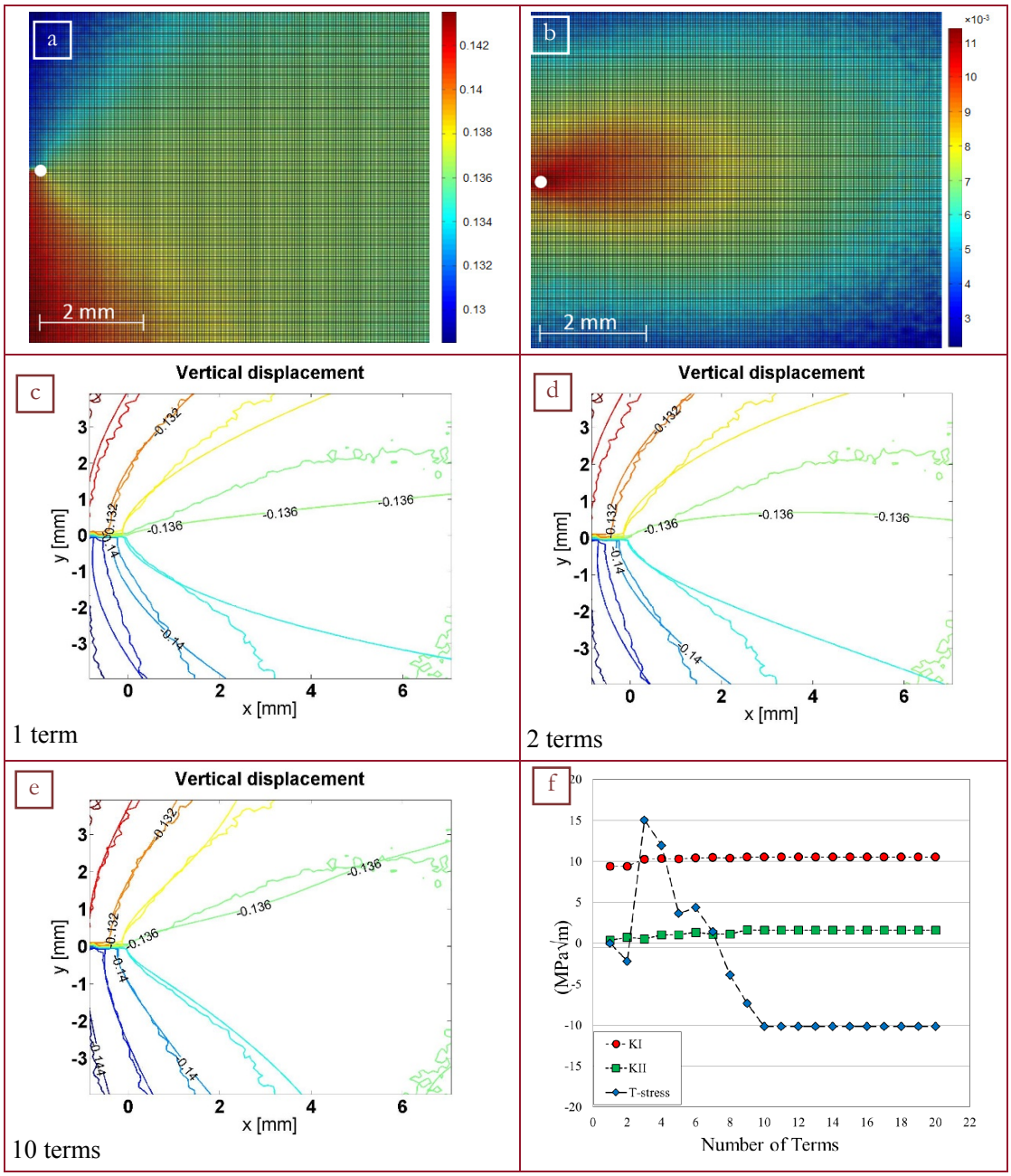

Figure 4. Analysed displacement field, a) vertical displacement, b) horizontal displacement. Fitting of displacement data to Williams' solution with one (c), two (d) and 10 terms (e) and stability of calculated SIF and T-stress for the first 20 terms of Williams' series (f).

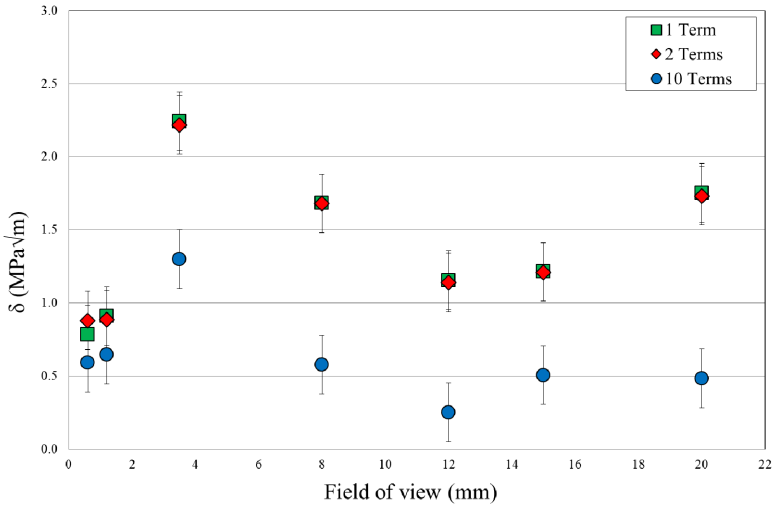

Figure 5. Difference between theoretical and experimental SIF, δ, as a function of FOV for different number of Williams' terms.

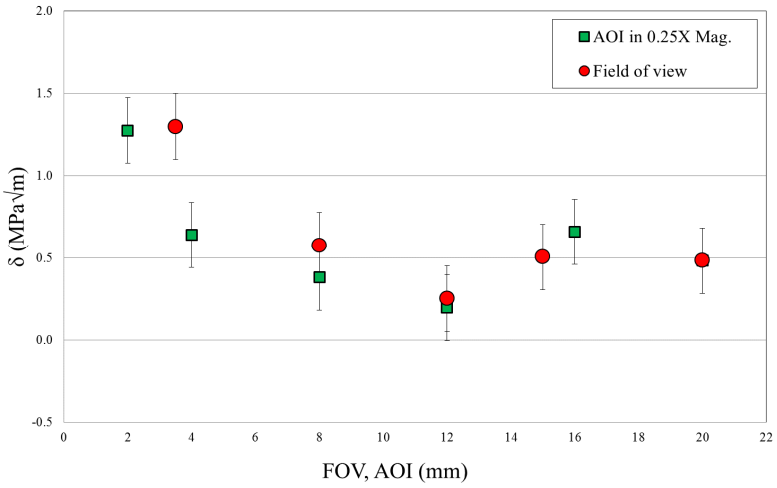

Figure 6. Comparison between the effect of the AOI and FOV on δ

ACKNOWLEDGEMENTS

Financial support of Junta de Andalucía through Proyectos de Excelencia grant reference TEP-3244; Spanish Ministerio de Economía y Competitividad through grant reference DPI2012-33382; and University of Malaga through Campus de Excelencia Internacional del Mar (CEIMAR) through Líneas Emergentes program and for providing PhD excahnge scholarship is greatly acknowledged.

REFERENCES

[1] Peters, W.H., Ranson, W.F., Kalthoff, J.F., Winkler, S.R., A Study of Dynamic near-Crack-Tip Fracture Parameters by Digital Image Analysis, Le Journal de Physique Colloques, 46(C5) (1985) C5-631-C635-638.

[2] Sutton, M.A., Mingqi, C., Peters, W.H., Chao, Y.J., McNeill, S.R., Application of an optimized digital correlation method to planar deformation analysis, Image and Vision Computing, 4(3) (1986) 143-150.

[3] Sutton, M.A., Wolters, W.J., Peters, W.H., Ranson, W.F., McNeill, S.R., Determination of displacements using an improved digital correlation method, Image and Vision Computing, 1(3) (1983) 133-139.
[4] Pan, B., Qian, K., Xie, H., Asundi, A., Two-dimensional digital image correlation for in-plane displacement and strain measurement: a review, Measurement Science and Technology, 20(6) (2009) 062001.
[5] Pan, B., Xie, H., Wang, Z., Qian, K., Wang, Z., Study on subset size selection in digital image correlation for speckle patterns, Optics express, 16(10) (2008) 7037-7048.
[6] Roux, S., Réthoré, J., Hild, F., Digital image correlation and fracture: an advanced technique for estimating stress intensity factors of 2D and 3D cracks, Journal of Physics D: Applied Physics, 42(21) (2009) 214004.
[7] Lopez-Crespo, P., Shterenlikht, A., Yates, J.R., Patterson, E.A., Withers, P.J., Some experimental observations on crack closure and crack-tip plasticity, Fatigue and fracture of engineering materials and structures, 32 (2009) 418-429.
[8] Yates, J.R., Zanganeh, M., Tai, Y.H., Quantifying crack tip displacement fields with DIC, Engineering Fracture Mechanics, 77(11) (2010) 2063-2076.
[9] Fazzini, M., Mistou, S., Dalverny, O., Robert, L., Study of image characteristics on digital image correlation error assessment, Optics and Lasers in Engineering, 48(3) (2010) 335-339.
[10] Schreier, H., Sutton, M., Systematic errors in digital image correlation due to undermatched subset shape functions, Experimental Mechanics, 42(3) (2002) 303-310.
[11] Schreier, H.W., Braasch, J.R., Sutton, M.A., Systematic errors in digital image correlation caused by intensity interpolation, Optical Engineering, 39(11) (2000) 2915-2921.
[12] Yu, L., Pan, B., The errors in digital image correlation due to overmatched shape functions, Measurement Science and Technology, 26 (2015) 045202-045202.
[13] Hild, F., Roux, S., Digital image correlation: from displacement measurement to identification of elastic properties–a review, Strain, 42(2) (2006) 69-80.
[14] Yoneyama, S., Ogawa, T., Kobayashi, Y., Evaluating mixed-mode stress intensity factors from full-field displacement fields obtained by optical methods, Engineering Fracture Mechanics, 74 (2007) 1399-1412.
[15] Lopez-Crespo, P., Shterenlikht, A., Patterson, E.A., Withers, P.J., Yates, J.R., The stress intensity of mixed mode cracks determined by digital image correlation, Journal of Strain Analysis for Engineering Design, (2008) 43.
[16] McNeill, S.R., Peters, W.H., Sutton, M.A., Estimation of stress intensity factor by digital image correlation, Engineering Fracture Mechanics, 28(1) (1987) 101-112.
[17] Hamam, R., Hild, F., Roux, S., Stress intensity factor gauging by digital image correlation: Application in cyclic fatigue, Strain, 43(3) (2007) 181-192.
[18] Lopez-Crespo, P., Burguete, R.L., Patterson, E.A., Shterenlikht, A., Withers, P.J., Yates, J.R., Study of a crack at a fastener hole by digital image correlation, Experimental Mechanics, 49 (2009) 551-559.
[19] Vasco-Olmo, J.M., Díaz, F.A., García-Collado, A., Dorado-Vicente, R., Experimental evaluation of crack shielding during fatigue crack growth using digital image correlation, Fatigue and Fracture of Engineering Materials and Structures, 38 (2015) 223-237.
[20] Vanlanduit, S., Vanherzeele, J., Longo, R., Guillaume, P., A digital image correlation method for fatigue test experiments, Optics and Lasers in Engineering, 47(3-4) (2009) 371-378.
[21] Sutton, M.A., Orteu, J.J., Schreier, H., Image Correlation for Shape, Motion and Deformation Measurements, (2009).
[22] American Society of T, Materials, Standard methods for the measurement of fatigue crack growth rates E647-95a, 03.01,1999. Annual Book of Standards, E647-95a. 1999;03.01.
[23] Murakami, Y., Stress Intensity Factors Handbook. Oxford: Pergamon Press, (1987).
[24] Sun, C.-T., Jin, Z.H., Fracture Mechanics. Academic Press, (2012).
[25] Soboyejo, W., Mechanical Properties of Engineered Materials. CRC Press, (2002).